Chemosphere 91 (2013) 248–257

Contents lists available at SciVerse ScienceDirect

Chemosphere

journal homepage: www.elsevier.com/locate/chemosphere

Upscaling retardation factor in hierarchical porous media with multimodal reactive mineral facies

Hailin Deng [a,*], Zhenxue Dai [a,1], Andrew V. Wolfsberg [a,2], Ming Ye [b,3], Philip H. Stauffer [a,4], Zhiming Lu [a,5], Edward Kwicklis [a,6]

[a] Earth and Environmental Sciences Division, Los Alamos National Laboratory, EES-16, T003, Los Alamos, NM 87545, United States
[b] Department of Scientific Computing and Geophysical Fluid Dynamics Institute, Florida State University, Tallahassee, FL 3230, United States

HIGHLIGHTS

- ▶ A new concept, reactive mineral facies to describe reactive mineral distribution.
- ▶ Using Lagrangian approach, the scale-dependent analytical expressions are derived.
- ▶ Describe scaling effect of effective retardation factor in time and space domains.

GRAPHICAL ABSTRACT

Concept model for reactive mineral facies at different spatial scales

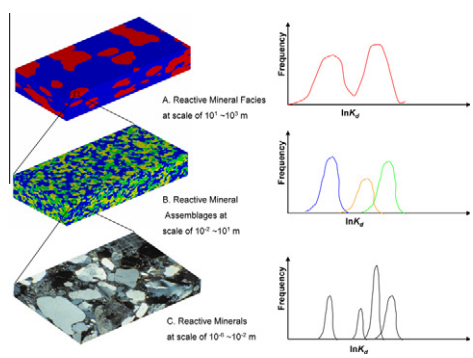

ARTICLE INFO

Article history:
Received 23 November 2011
Received in revised form 29 October 2012
Accepted 31 October 2012
Available online 20 December 2012

Keywords:
Upscaling
Retardation factor
Reactive mineral facies
Hierarchical porous media

ABSTRACT

Aquifer heterogeneity controls spatial and temporal variability of reactive transport parameters and has significant impacts on subsurface modeling of flow, transport, and remediation. Upscaling (or homogenization) is a process to replace a heterogeneous domain with a homogeneous one such that both reproduce the same response. To make reliable and accurate predictions of reactive transport for contaminant in chemically and physically heterogeneous porous media, subsurface reactive transport modeling needs upscaled parameters such as effective retardation factor to perform field-scale simulations. This paper develops a conceptual model of multimodal reactive mineral facies for upscaling reactive transport parameters of hierarchical heterogeneous porous media. Based on the conceptual model, covariance of hydraulic conductivity, sorption coefficient, flow velocity, retardation factor, and cross-covariance between flow velocity and retardation factor are derived from geostatistical characterizations of a three-dimensional unbounded aquifer system. Subsequently, using a Lagrangian approach the scale-dependent analytical expressions are derived to describe the scaling effect of effective retardation factors

* Corresponding author. Present address: CSIRO Land and Water, Private Bag No. 5, Wembley WA 6913, Australia. Tel.: +61 4 52196874.
E-mail addresses: hailin@lanl.gov (H. Deng), daiz@lanl.go (Z. Dai), awolf@lanl.gov (A.V. Wolfsberg), mye@fsu.edu (M. Ye), stauffer@lanl.go (P.H. Stauffer), zhiming@lanl.gov (Z. Lu), kwicklis@lanl.gov (E. Kwicklis).
[1] Tel.: 505 665 6387.
[2] Tel.: 505 667 3599.
[3] Tel.: 850 644 4587.
[4] Tel.: 505 665 4638.
[5] Tel.: 505 665 2126.
[6] Tel.: 505 665 7408.

0045-6535/$ - see front matter Published by Elsevier Ltd.
http://dx.doi.org/10.1016/j.chemosphere.2012.10.105

Nomenclature

a, b	constants in linear correlation between K and K_d (i.e. $\ln K_d = a \ln K + b$)
$C_{ff}(\xi)$	covariance function of $\ln K$
$C_{v_1R}(\xi)$	cross-covariance function of v_1 and R
$C_{v_1v_1}(\xi)$	covariance function of v_1
$C_{RR}(\xi)$	covariance function of R
f	perturbation of $\ln K$
$I_j(\mathbf{x})$	indicator variable of the j-th reactive mineral assemblage
J	mean hydraulic gradient oriented in x_1 direction
$\mathbf{k}$	a three-dimension wave-number vector, $\mathbf{k} = (k_1, k_2, k_3)^T$
K	hydraulic conductivity
K^G	geometric mean of $\ln K$ expressed as $\exp(M_Y)$
K_d	Sorption coefficient
K_d^G	geometric mean of $\ln K_d$
m_j	mean of the j-th reactive mineral assemblage
M_Y	composite mean of a random variable
n	porosity of medium
p_j	volumetric proportion of the j-th reactive mineral assemblage
r	perturbation of $\ln K_d$
R	retardation factor
R'	perturbation of retardation factor
$\mathbf{R}(\mathbf{x})$	retardation factor as a function of spatial location
$\tilde{R}(x)$	scale dependent effective retardation factor
$\tilde{R}(t)$	time dependent effective retardation factor
$\overline{R}$	mean retardation factor
$S_{RR}(\mathbf{k})$	spectrum density of retardation factor
$S_{rr}(\mathbf{k})$	spectrum density of the fluctuations of $\ln K_d$
$S_{ff}(\mathbf{k})$	spectrum density of the fluctuations of $\ln K$
$S_{fr}(\mathbf{k})$	cross spectrum density of $\ln K$ and $\ln K_d$
$S_{v_1v_1}(\mathbf{k})$	spectrum density of flow velocity
$S_{v_1R}(\mathbf{k})$	cross spectrum density of v_1 and R
T	travel time for a sorbing solute
T_p	travel time for a conservative solute
$\mathbf{u}(\mathbf{x})$	Eulerian solute velocity
$\tilde{u}(t)$	time dependent effective solute velocity
v_1'	perturbation of flow velocity
$\overline{v}_1$	mean flow velocity
$\mathbf{v}(\mathbf{x})$	Eulerian flow velocity
$\mathbf{x}$	spatial coordinator vector
$Y(\mathbf{x})$	multimodal spatial random variable for K, K_d or R
$Y_j(\mathbf{x})$	random variable of the j-th reactive mineral assemblage
ξ	separation distance or lag distance
σ_Y^2	composite variance of a random variable
σ_j^2	variance of the j-th reactive mineral assemblage
$\sigma_{v_1R}^2$	cross-variance of flow velocity and retardation factor
$\sigma_{v_1}^2$	variance of flow velocity
σ_R^2	variance of retardation factor
ρ_b	bulk density of medium
λ_i	correlation length of the i-th reactive mineral assemblage
λ_I	indicator correlation length

in temporal and spatial domains. When time and space scales become sufficiently large, the effective retardation factors approximate their composite arithmetic mean. Correlation between the hydraulic conductivity and the sorption coefficient can significantly affect the values of the effective retardation factor in temporal and spatial domains. When the temporal and spatial scales are relatively small, scaling effect of the effective retardation factors is relatively large. This study provides a practical methodology to develop effective transport parameters for field-scale modeling at which remediation and risk assessment is actually conducted. It does not only bridge the gap between bench-scale measurements to field-scale modeling, but also provide new insights into the influence of hierarchical mineral distribution on effective retardation factor.

Published by Elsevier Ltd.

1. Introduction

Estimation of effective transport parameters in physically and chemically heterogeneous geological media has received growing amount of attention in the past decade (Rubin, 2003; Davis et al., 2004). Numerous investigations show that the transport parameters are spatially and/or temporally scale-dependent in both porous and fractured media (e.g. Rajaram, 1997; Liu et al., 2008; Dai et al., 2009). These studies indicate that the scale dependence is originated from physical and chemical heterogeneity of sediments. For transport of a reactive solute with linear equilibrium adsorption, spatial variability of the sorption coefficients (K_d) has significant effect on retardation factors (R) because of the linear relationship of $R = 1 + (\rho_b/n)K_d$, where ρ_b and n are bulk density and porosity of the medium, respectively. Spatial distributions of K_d for reactive solutes in sediments are heterogeneous (Allen-King et al., 2006). The dilemma in reactive transport modeling is that measurements of sorption coefficients are often obtained from small-scale column experiments (Cheng et al., 2007) while contaminant remediation and risk assessment are actually conducted at larger field scales. Therefore, to bridge the scale gaps and to estimate effective transport parameters for field-scale modeling, we need transfer of knowledge obtained at column scale to a larger field scale through upscaling, which is one of the most important processes for field-scale transport modeling.

The sorption coefficient and hydraulic conductivity are spatially correlated in sediments (Allen-King et al., 2006). Using a sedimentary facies-based geostatistical approach, Allen-King et al. (1998) described the heterogeneous distributions of perchloroethene (PCE) K_d and hydraulic conductivity (K) and their spatial correlation at the Borden site; significantly positive correlations between K_d and K were found within and between different facies. Using a Lagrangian approach, Rajaram (1997) derived analytical expressions for scale-dependent effective retardation factor in unimodal porous media by assuming various spatial correlations between K_d and K. Deng et al. (2010) applied dual-porosity model and concept of reactive mineral facies describing multimodal fractured porous media and upscaled tortuosity and retardation factor for reactive transport. Attinger et al. (1999) reported time behavior of solute cloud in chemically heterogeneous porous media with a space-dependent retardation factor using

stochastic method within Fourier transformation domain. More studies on the scaling of R in unimodal porous media can be found in Chrysikopoulos et al. (1990), Bellin et al. (1993), Cvetkovic and Dagan (1994) and Fernàndez-Garcia et al. (2005).

Continuous time random walk (CTRW) has been proposed as a new theoretical framework for upscaling retardation factor and investigating anomalous transport (non-Fickian transport) in geological porous media (Berkowitz et al., 2006). Using CTRW, Dentz et al. (2004) explored time behavior of effective solute transport in heterogeneous porous media, particularly the transition from anomalous to normal transport. An interesting and significant result given by Dentz and Castro (2009) based on CTRW formulation, displayed that in porous media with heterogeneously distributed retardation an (constant) effective retardation factor may not always exist at practically relevant time and length scales. Dentz and Boster (2010) identified two different mechanisms causing anomalous transport in quenched random porous media due to different heterogeneities between broad disorder point distribution and strong disorder correlations. Bolster and Dentz (2012) further studied anomalous dispersion in heterogeneous porous media with a spatially varying retardation factor and derived effective transport equation in a complex Fourier–Laplace space. It is also worthy to point out that the definition of retardation factor used in CTRW framework is different from that in traditional advection–dispersion transport equation.

Mineral facies is the physical and chemical basis for describing the correlation between hydraulic conductivity and sorption coefficient. Geological formations consist of various minerals and organic materials, which can be grouped into different types of facies. For fluid flow and conservative solute transport, the sedimentary facies-based characterizations can appropriately represent multimodal conductivity distributions because variability of the sedimentary facies accurately reflects the physical controls of conductivity and flow velocity (Ritzi et al. (2004), Dai et al., 2004). For transport of a reactive solute in porous media, the sedimentary facies-based conceptual model does not always work well because the sedimentary facies does not always capture the chemical heterogeneity of the sorption coefficients (Allen-King et al., 1998). In porous media the values of sorption coefficients are mainly controlled by reactive minerals (Cheng et al., 2007) including organic carbon (Russo et al., 2010), which are distinguished as any mineral or mineral facies controlling one or a group of specified sorption reactions (e.g., Allen-King et al., 2006). This renders a multimodal for the sorption coefficients. Therefore, a reactive mineral facies-based conceptual model is conceived in this study for characterizing the physical and chemical heterogeneity in porous media.

This study focuses on upscaling the retardation factor for reactive solute transport in multimodal reactive mineral facies (RMFs) that consist of a porous medium. It is different from method used by Russo et al. (2010), which is based on nonlinear, rate-limited sorption/desorption with a continuous distribution function. A conceptual model of RMFs is first described for the heterogeneous porous media with hierarchical structures, followed by geostatistic characterization of random variables R and flow velocity. Then, the temporally and spatially scale-dependent equations of effective retardation factors are derived using a Lagrangian approach coupled with transition probability models, followed by discussions and conclusions.

2. Conceptual model for hierarchical multimodal porous media

Sorption reactions in porous media depend not only on aqueous-phase chemical species and physiochemical conditions (e.g., temperature, oxygen fugacity, pH, and Eh) but also on types of reactive minerals (RMs) and their spatial distributions. From small to large scales, the RMs constitute reactive mineral assemblages (RMAs), which in turn form reactive mineral facies (RMFs). A conceptual model of the RMFs in quartz-feldspar sandstone is constructed for reactive transport in heterogeneous porous media with multimodal K_d and K. As described in Fig. 1, the spatial distributions of uranium sorption coefficients are characterized at each hierarchical level (For convenience of discussion, the species uranium is used as an example).

RM at the microform scale (10^{-6} to 10^{-2} m) refers to any minerals that are sensitive to a specified geochemical reaction. As shown by the four probability distributions of $\ln K_d$ in Fig. 1C, different RMs such as calcite, smectite, hematite and organic matters usually have different sorption coefficients for uranium. Quartz and feldspar are not considered as RMs in the sandstone because their sorption coefficients for the uranium are extremely low. However, these non-reactive minerals (NRMs) occupy a large volumetric proportion of the rock; the spatial distributions of NRMs can thus result in heterogeneous patterns of the RMs and in turn affect the statistical properties (e.g. proportion and correlation length) of the RMs.

A RMA at the mesoform scale (10^{-2} to 10^{1} m) represents coexisting of NRMs and RMs for a specified geochemical reaction. Because of different statistical distributions of the uranium sorption coefficients among different RMs (Fig. 1A), three different RMAs, i.e. Clay-Quartz-feldspar, Clay-Fe_2O_3-Quartz-Feldspar, and Clay-Organic Mater-Quartz-Feldspar, may have different statistical distributions of uranium sorption coefficients (Fig. 1B). In other words, if different RMs have significantly different statistical distributions of the uranium sorption coefficients, the RMA composed of the RMs will have a multimodal structure for the uranium sorption coefficients (Fig. 1B and Table 1). Given that there can be one or several non-reactive mineral assemblages (NRMAs), the spatial distributions of NRMAs among RMAs can also affect the spatial heterogeneity of RMA distributions in the sandstone.

A RMF is a body of rock that is characterized by an association of RMAs (or RMAs and NRMAs) for a specified geochemical reaction. Due to temporal and spatial variability of sedimentation, weathering and oxidation of sandstones, the spatial distributions of RMAs are heterogeneous. Two types of RMFs, i.e. Calcite-Clay-Organic Matter RFM (CCO-RMF) and Clay-Hematite RFMs (Fig. 1C), are summarized in this study on intensity of oxidation and degrees to which the RMF influence uranium sorption in the sandstone. For the purpose of demonstration, only the CCO-RMF is used for upscaling from three RMAs in this study, and flow and transport are assumed to occur in CCO-RMF. Upscaling the reactive transport parameters from the RMF scale to a larger scale can be easily extended, but is beyond the scope of this study.

This conceptual model of the hierarchical structure of the RMFs provides a basis for upscaling the sorption coefficient. After all appropriate RMFs are identified and their hierarchical structure is established, multimodal cross-covariance functions are developed for upscaling the retardation factor using indicator geostatistics and a transition probability model (e.g., Dai et al., 2007a) to describe the distribution patterns of RMAs.

3. Geostatistical characterization of random variables in multimodal porous media

Although the conceptual model above contains the three hierarchical levels of the K and K_d, for the purpose of demonstration, the upscaling equations developed below are only for two levels, i.e. from the RMA to the RMF. These equations can be easily extended to any number of hierarchical levels as suggested in Dai et al. (2004). Consider a domain Ω filled with N RMA of mutually exclusive occurrences. Let $Y(\mathbf{x})$ be multimodal spatial random variables for K, K_d or R at location $\mathbf{x}$. It can be expressed via indicator geostatistics as:

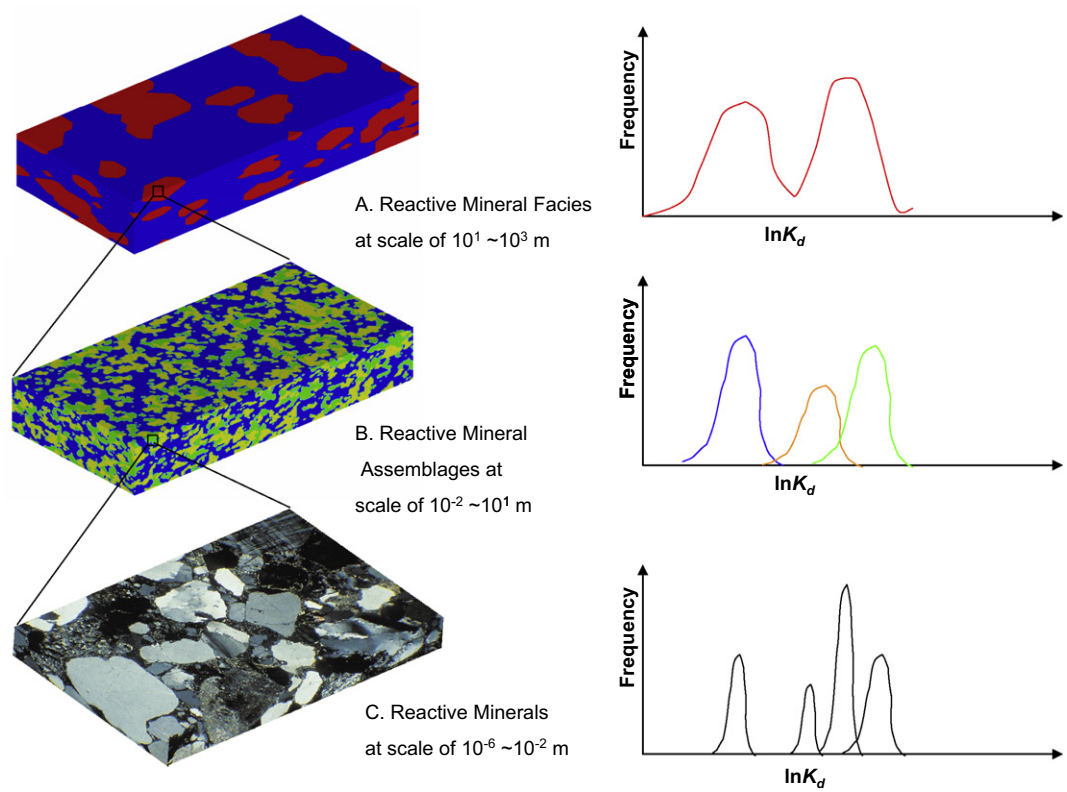

Fig. 1. Concept model for reactive mineral facies at different spatial scales.

$$Y(\mathbf{x}) = \sum_{j=1}^{N} I_j(\mathbf{x}) Y_j(\mathbf{x}), \tag{1}$$

where $I_j(\mathbf{x})$ is indicator variable within the domain Ω and $Y_j(\mathbf{x})$ are the random variables of the j-th RMA. Following Ritzi et al. (2004), the composite mean M_Y and variance σ_Y^2 of the random variable are computed via:

$$M_Y = \sum_{j=1}^{N} p_j m_j, \tag{2}$$

$$\sigma_Y^2 = \sum_{j=1}^{N} p_j \sigma_j^2 + \frac{1}{2} \sum_{i=1}^{N} \sum_{j=1}^{N} p_i p_j (m_i - m_j)^2, \tag{3}$$

where p_j, m_j and σ_j^2 are volumetric proportion, mean and variance, respectively. Consider a steady groundwater flow in a three dimensional unbounded porous medium with a mean hydraulic gradient (J) oriented in x_1 direction. Similar to the method used by Rajaram (1997), we assume that the hydraulic conductivity K is also second-order stationary and log normal distributed. For reactive solute transport in such a porous medium, the solute velocity u and retardation factor R are assumed to be second-order stationary, and that the sorption coefficient K_d follows a log normal distribution. Following Gelhar (1993) and Rajaram (1997), perturbations of R and v_1 are obtained as:

$$R' = \frac{\rho_b}{n} K_d^G r, \tag{4}$$

$$v_1' = \frac{K^G J}{n} \left(1 - \frac{k_1^2}{k^2}\right) f, \tag{5}$$

where the prime symbol indicates pertubations, superscript G denotes geometric mean expressed as $\exp(M_Y)$, r and f are pertubations of $\ln K_d$ and $\ln K$, respectively. Therefore the spectrum densities of the retardation factor and flow velocity are expressed as below:

$$S_{RR}(\mathbf{k}) = \left(\frac{\rho_b}{n} K_d^G\right)^2 S_{rr}(\mathbf{k}), \tag{6}$$

$$S_{v_1 v_1}(\mathbf{k}) = \frac{1}{n^2} (K^G J)^2 \left(1 - \frac{k_1^2}{k^2}\right)^2 S_{ff}(\mathbf{k}), \tag{7}$$

where S_{ff} and S_{rr} are the spectral density of the fluctuations of $\ln K$ and $\ln K_d$, respectively, and $\mathbf{k} = (k_1, k_2, k_3)^T$ is a 3-D wave-number vector. If K and K_d are perfectly correlated as $\ln K_d = a \ln K + b$, where a and b are real constants, then the cross spectrum of $\ln K$ and $\ln K_d$ has a linear relationship with the spectrum of $\ln K$, i.e. $S_{fr}(\mathbf{k}) = aS_{ff}(\mathbf{k})$ and the cross spectrum density of v_1 and R is expressed as (Rajaram, 1997):

$$S_{v_1 R}(\mathbf{k}) = \frac{\rho_b}{n^2} K_d^G K^G J a \left(1 - \frac{k_1^2}{k^2}\right) S_{ff}(\mathbf{k}). \tag{8}$$

Using the relationship between the spectrum and the covariance function yields:

$$S_{ff}(\mathbf{k}) = \frac{1}{(2\pi)^3} \iiint_{-\infty}^{\infty} e^{-i\mathbf{k}\cdot\xi} C_{ff}(\xi) d\xi, \tag{9}$$

where ξ is separation distance or lag distance. For the multimodal covariance function of $\ln K$, we can assume that it follows an exponential form (Dai et al., 2007b), i.e.

Table 1
Synthetic parameters of three RMA used for model calculation and plotting.

RMF	RMA	L_j	p_j	Parameter	m_j	σ_j^2	M_j^G	λ_j	λ_ψ	R_j
Cc-Clay-OM RMF	Cc-QF	50	0.6	$\ln K$	1.5	0.6	4.48	10	6.67	2.39
				$\ln K_d$	−2.2	0.22	0.11	12	7.5	
	Clay-Fe_2O_3-QF	23.5	0.15	$\ln K$	0.5	0.3	1.65	6	4.62	4.76
				$\ln K_d$	−1.2	0.12	0.3	8	5.71	
	Clay-OM-QF	26.7	0.25	$\ln K$	0.05	0.15	1.05	9	6.21	10.26
				$\ln K_d$	−0.3	0.1	0.74	7	5.19	
	Parameters	$\ln K$			$\ln K_d$			R		
	Statistics	M_Y	σ_Y^2	M_Y^G	M_Y	σ_Y^2	M_Y^G	M_Y	σ_Y^2	M_Y^G
	Values	0.99	0.86	2.68	−1.58	0.84	0.21	4.93	5.6	3.59
	Parameters	$\bar{v}_1$	$\sigma_{v_1R}^2$	λ_I	n	ρ_b	J			
	Values	0.21	0.2	20	0.2	2.5	0.01			

Note: RMA = reactive mineral assemblage, Cc = calcite, Fe_2O_3 = iron oxides, QF = quartz and feldspar; For j-th RMA (j = 1, 2, 3), L_j = mean length (m), M_j^G = geometric mean, λ_j = correlation length (m), $\lambda_\psi = \lambda_j\lambda_I/(\lambda_j + \lambda_I)$, R_j = retardation factor; M_Y = global mean, σ_Y^2 = global variance, M_Y^G = global geometric mean, $\bar{v}_1$ = mean flow velocity (m d^{-1}), $\sigma_{v_1R}^2$ = cross covariance of flow velocity and retardation factor, λ_I = indicator correlation length (m), n = porosity, ρ_b = bulk density of the porous media (g cm^{-3}), J = average hydraulic gradient, K = hydraulic conductivity (m d^{-1}), K_d = sorption coefficient (cm^3 g^{-1}).

$$C_{ff}(\xi) = \sum_{i=1}^{N} p_i^2\sigma_i^2 e^{-\eta_1} + \sum_{i=1}^{N} p_i(1-p_i)\sigma_i^2 e^{-\eta_2} + \frac{1}{2}\sum_{i=1}^{N}\sum_{j=1}^{N} p_i p_j (m_i - m_j)^2 e^{-\eta_3}, \tag{10}$$

where $\eta_1 = \lambda_i/\xi$, $\eta_2 = \lambda_\psi/\xi$, and $\eta_3 = \lambda_I/\xi$ are the dimensionless distances. λ_i and λ_I are the correlation length of i-th RMA and the indicator correlation length for the whole domain, respectively; $\lambda_\psi = \lambda_i\lambda_I/(\lambda_i + \lambda_I)$, and N is the number of RMA in the multimodal porous medium. Substituting (10) into (9) and integrating (9), the spectrum corresponding to the multimodal covariance function is obtained as:

$$S_{ff}(\mathbf{k}) = \left\{ \sum_{i=1}^{N} p_i^2 \frac{\sigma_i^2\lambda_i^3}{\pi^2(1+k^2\lambda_i^2)} + \sum_{i=1}^{N} p_i(1-p_i)\frac{\sigma_i^2\lambda_\psi^3}{\pi^2(1+k^2\lambda_\psi^2)} + \frac{1}{2}\sum_{i=1}^{N}\sum_{j=1}^{N} p_i p_j (m_i - m_j)^2 \frac{\lambda_I^3}{\pi^2(1+k^2\lambda_I^2)} \right\}. \tag{11}$$

Integration method used for Eq. (9) can be found in Appendix A. Then substituting (11) into (8), using the relationship between the spectrum and the covariance function and integrating (8) over wave number space, the cross-covariance of v_1 and R for the multimodal isotropic porous medium is:

$$\begin{aligned} C_{v_1R}(\xi) &= \int\int_{-\infty}^{\infty}\int e^{i\mathbf{k}\cdot\xi} S_{v_1R}(\mathbf{k})d\mathbf{k} \\ &= \frac{\rho_b}{n^2}K_d^G K^G Ja\left\{ \sum_{i=1}^{N} p_i^2\sigma_i^2 F_1(\eta_1) + \sum_{i=1}^{N} p_i(1-p_i)\sigma_i^2 F_1(\eta_2) + \frac{1}{2}\sum_{i=1}^{N}\sum_{j=1}^{N}(m_i - m_j)^2 p_i p_j F_1(\eta_3) \right\}, \end{aligned} \tag{12}$$

where $F_1(\eta) = 4\eta^3(1 - e^{-\eta}) - 2\eta e^{-\eta} - 4\eta^2 e^{-\eta}$. If the separation distance approaches to zero, the cross-covariance of the v_1 and R is:

$$\sigma_{v_1R}^2 = \frac{2\rho_b}{3n^2}K_d^G K^G Ja\left\{ \sum_{i=1}^{N} p_i\sigma_i^2 + \frac{1}{2}\sum_{i=1}^{N}\sum_{j=1}^{N} p_i p_j (m_i - m_j)^2 \right\}, \tag{13}$$

Integration method used to attain Eqs. (12), (13) can be found in Appendix B. Similarly, using Eq. (7) and the relationship between the spectrum and the covariance function, and then integrating produces the covariance of v_1, i.e.,

$$C_{v_1v_1}(\xi) = \frac{(K^G J)^2}{n^2}\left\{ \sum_{i=1}^{N} p_i^2\sigma_i^2 F_2(\eta_1) + \sum_{i=1}^{N} p_i(1-p_i)\sigma_i^2 F_2(\eta_2) + \frac{1}{2}\sum_{i=1}^{N}\sum_{j=1}^{N}(m_i - m_j)^2 p_i p_j F_2(\eta_3) \right\}, \tag{14}$$

where $F_2(\eta) = [8\eta^2 + 48\eta^3 + 96\eta^4]e^{-\eta} + [96\eta^5 - 8\eta^3](e^{-\eta} - 1)$ .Thus the variance of $v_1$can be retrieved as the dimensionless distances $\eta \to \infty$:

$$\sigma_{v_1}^2 = \frac{8}{15}\frac{(K^G J)^2}{n^2}\left\{ \sum_{i=1}^{N} p_i\sigma_i^2 + \frac{1}{2}\sum_{i=1}^{N}\sum_{j=1}^{N} p_i p_j (m_i - m_j)^2 \right\}, \tag{15}$$

In the same way, the multimodal covariance of R is obtained according to Eq. (6), i.e.

$$C_{RR}(\xi) = \left(\frac{\rho_b}{n}K_d^G\right)^2\left\{ \sum_{i=1}^{N} p_i^2\sigma_{ri}^2 e^{-\eta_1} + \sum_{i=1}^{N} p_i(1-p_i)\sigma_{ri}^2 e^{-\eta_2} + \frac{1}{2}\sum_{i=1}^{N}\sum_{j=1}^{N} p_i p_j (m_{ri} - m_{rj})^2 e^{-\eta_3} \right\}, \tag{16}$$

where σ_{ri}^2 and m_{ri} are the variance and mean of $\ln K_d$ of the i-th RMA, respectively, λ_{ri} is correlation length of $\ln K_d$ for the i-th RMA. Therefore, the corresponding variance of retardation factors is

$$\sigma_R^2 = \left(\frac{\rho_b}{n}K_d^G\right)^2\left\{ \sum_{i=1}^{N} p_i\sigma_{ri}^2 + \frac{1}{2}\sum_{i=1}^{N}\sum_{j=1}^{N} p_i p_j (m_{ri} - m_{rj})^2 \right\}, \tag{17}$$

The covariance and cross-covariance derived here will be applied in the following development of time- and scale-dependent retardation factors for the multimodal porous media.

4. Time dependent effective retardation factor

For reactive solute transport with linear equilibrium sorption in a 3-D unbound saturated porous medium, the Eulerian solute velocity is defined as $\mathbf{u}(\mathbf{x}) = \mathbf{v}(\mathbf{x})/\mathbf{R}(\mathbf{x})$ with a spatially variable retardation factor $\mathbf{R}(\mathbf{x})$. Using the assumptions made in Section 3 that u, v and R are all second order stationary, the effective retardation factor in non-dimensional form is thus expressed as (Rajaram, 1997)

$$\tilde{R}(t) = \bar{v}_1/\tilde{u}(t), \tag{18}$$

where upper bar indicates mean, and upper tilde denotes effective value. Then Lagrangian mean velocity of a reactive solute is described as $u_i(\mathbf{X}_t) = dX_{ti}/dt$, where X_{ti} means the component of posi-

tion vector in the direction i-th (i = 1, 2, or 3). In the Lagrangian framework, Rajaram (1997) developed an equation for the time dependent effective retardation factor, $\tilde{R}(t)$, as:

$$\frac{\overline{R}}{\tilde{R}(t)} = \left(1 + \frac{\sigma_R^2}{\overline{R}^2} - \frac{\sigma_{v_1R}^2}{\bar{v}_1\overline{R}}\right) - \frac{\tilde{R}(t)}{\overline{R}}\left\{\frac{1}{\overline{R}^2}[\sigma_R^2 - C_{RR}(\xi,0,0)] - \frac{1}{\bar{v}_1\overline{R}}[\sigma_{v_1R}^2 - C_{v_1R}(\xi,0,0)]\right\}, \quad (19)$$

where separation distance $\xi = \bar{v}_1 t/\tilde{R}(t)$. Eq. (19) shows that the behavior of $\tilde{R}(t)$ is determined by the covariance (C_{RR}) and cross-covariance (C_{v_1R}). Substituting the multimodal covariance (16) and cross-covariance (12) into (19), $\tilde{R}(t)$ can be evaluated. For the multimodal porous media, when the solute travel time (t) approaches to infinity, $\overline{R}/\tilde{R}(\infty) = 1$, indicating that $\tilde{R}(t)$ approaches the arithmetic average of R, which is similar to the result of Rajaram (1997) for unimodal porous media. As $t \to 0$, the following equation holds:

$$\frac{\overline{R}}{\tilde{R}(t)} = \left(1 + \frac{\sigma_R^2}{\overline{R}^2} - \frac{\sigma_{v_1R}}{\bar{v}_1\overline{R}}\right). \quad (20)$$

5. Space dependent effective retardation factor

In the 3-D random velocity field, the uniform mean flow direction is parallel to the x_1-direction. When a solute particle started traveling at the origin in the 3-D field, the ensemble average of the travel time through the x_2–x_3 plane at a distance x from the origin is expressed by $T(x)$. According to Dagan et al. (1992) and Rajaram (1997), the differential equation of $T(x)$ for a sorbing particle is:

$$\frac{dT}{dx} = \frac{\overline{R}}{\bar{v}_1}\left[1 + \frac{1}{\bar{v}_1^2}C_{v_1v_1}(x,0,0) - \frac{1}{\overline{R}\bar{v}_1}C_{v_1R}(x,0,0)\right] \quad (21)$$

For a conservative solute particle, R is equal to 1. After integration, Eq. (21) becomes:

$$T_p = \frac{x}{\bar{v}_1} + \frac{(K^GJ)^2}{\bar{v}_1^3 n^2}\left\{\sum_{i=1}^{N} p_i^2\sigma_i^2\lambda_i G_1(\beta_1) + \sum_{i=1}^{N} p_i(1-p_i)\sigma_i^2\lambda_{\psi i}G_1(\beta_2) + \frac{1}{2}\sum_{i=1}^{N}\sum_{j=1}^{N}(m_i - m_j)^2 p_i p_j \lambda_I G_1(\beta_3)\right\} \quad (22)$$

where $G_1(\beta) = 24\beta^4(1-e^{-\beta}) - 24\beta^3 e^{-\beta} - 4\beta^2(1+2e^{-\beta}) + 1$; $\beta_1 = \lambda_i/x$, $\beta_2 = \lambda_\psi/x$, and $\beta_3 = \lambda_I/x$ are the dimensionless distances. Similarly, for a sorbing particle, substituting (12) and (14) into Eq. (21) and integrating over x obtain:

$$T = \overline{R}T_p - \frac{\rho_b K_d^G K^G Ja}{n^2\bar{v}_1^2}\left\{\sum_{i=1}^{N} p_i^2\sigma_i^2\lambda G_2(\beta_1) + \sum_{i=1}^{N} p_i(1-p_i)\sigma_i^2\lambda_{\psi i}G_2(\beta_2) + \frac{1}{2}\sum_{i=1}^{N}\sum_{j=1}^{N}(m_i - m_j)^2 p_i p_j \lambda_I G_2(\beta_3)\right\} \quad (23)$$

where $G_2(\beta) = 2\beta^2(e^{-\beta} - 1) + 2\beta e^{-\beta} + 1$. Integration method used for Eqs. (22), (23) can be found in Appendix C. Finally, the scale dependent effective R for isotropic multimodal porous media is computed by:

$$\tilde{R}(x) = T/T_p, \quad (24)$$

6. Discussion and conclusions

In order to illustrate the scale dependence of retardation factors with the above derived equations, we build a synthetic example in which the parameter values of the three RMAs are extracted from a real case (see Table 1). The time-dependent effective R for the RMF is plotted in Fig. 2A for three cases of correlations between K and K_d: positively correlated (a = 1), uncorrelated (a = 0), and negatively correlated (a = −1). In all three cases, the effective R increases monotonically with time, but starting with different values and at different growth rates. Fig. 2A shows that the effective R values of the two correlated are larger than that of uncorrelated case, in particular in the early time due to contribution from the cross-covariance between v_1 and R (Eq. (12)). As expected, the effective R in the three cases converges to the arithmetic mean of R when time is sufficiently large.

Spatial variation of the effective R is plotted in Fig. 2B for the three cases with the same parameters given in Table 1. In the uncorrelated case the effective R keeps constant, whereas in case of the positive correlation the effective R rapidly increases within the distance of 100 m and then gradually increases with distance. In the case of negative correlation, the effective R rapidly decreases at the first 100 m, and then gradually decreases with distance. For both positive and negative correlation cases, however, the effective R approaches to the arithmetic mean when the distance is sufficiently large.

Fig. 2C shows the time-dependent effective R changes with the indicator correlation length (λ_I) when the time is fixed at 1000 d. In the case of positive correlation, the effective R increases to a maximum at about 15 m, and then gradually decreases until λ_I reaches 1000 m, and finally decreases slowly with λ_I. In the case of negative correlation, the effective R reaches its maximum at λ_I = 200 m, and then gradually decreases until it approximates to a minimum at λ_I > 10000 m. Under the situation of non-correlation, the effective R keeps constant until λ_I = 100 m, then gradually decreases with λ_I until reaching its minimum at about 50000 m. Although the effective R decreases to a minimum for three cases, it reaches to different minimums. This reflects the different contribution from the cross-covariance function. Fig. 2D reveals the spatial scale-dependent effective R increases with λ_I in the case of negative correlation, but decreases with λ_I in the case of positive correlation. If there is no correlation between K and K_d, the effective R does not changes with λ_I.

Fig. 3 shows that the scale-dependent effective retardation factors do not change much with variances of the hydraulic conductivity. However, they do change greatly with variances of the sorption coefficients, especially when the variances are larger than 0.1 for RMA 1 and great than 0.3 for RMA 2 (Fig. 4).

Our results above focus on methodology for upscaling retardation factor, which is different from the study of Dentz and Castro (2009). They derived an analytical expression for effective transport equation based on CTRW formulation, which describes the behavior of the ensemble averaged concentration of a sorping solute. Dentz and Boster (2010) employed a three-step method to average two types of anomalous transport. This two studies did not formulate effective retardation factor while they developed effective transport equations. Direct comparison of our results with theirs is beyond the scope of this paper. In future, using our equations of effective retardation factor to model reactive transport can be directly compared with the results of Dentz and Castro (2009) and Dentz and Boster (2010).

When collating our study with those by Dentz and Castro (2009) and Bolster and Dentz (2012), we noticed that our definition of retardation factor is different from theirs in CTRW. Ours is derived from traditional advection–dispersion equation (ADE). It is defined as $R = 1 + (\rho_b/n)K_d$. Dentz and Castro (2009) defined the retardation factor (they called retardation coefficient) as $R = [n + (1-n)K_d]/\bar{n}$ while Bolster and Dentz (2012) gave another definition for retardation factor, $R = 1 + K_d$. It is not clear that how different modeling results can be caused by different definitions of retardation factor.

In general, this study shows from a new theoretical angle that the correlation between K and K_d can significantly affect the effective R in temporal and spatial domain. The temporal and spatial scale-dependent R originated from the physical and chemical heterogeneity and the correlation of K and K_d. When the temporal and

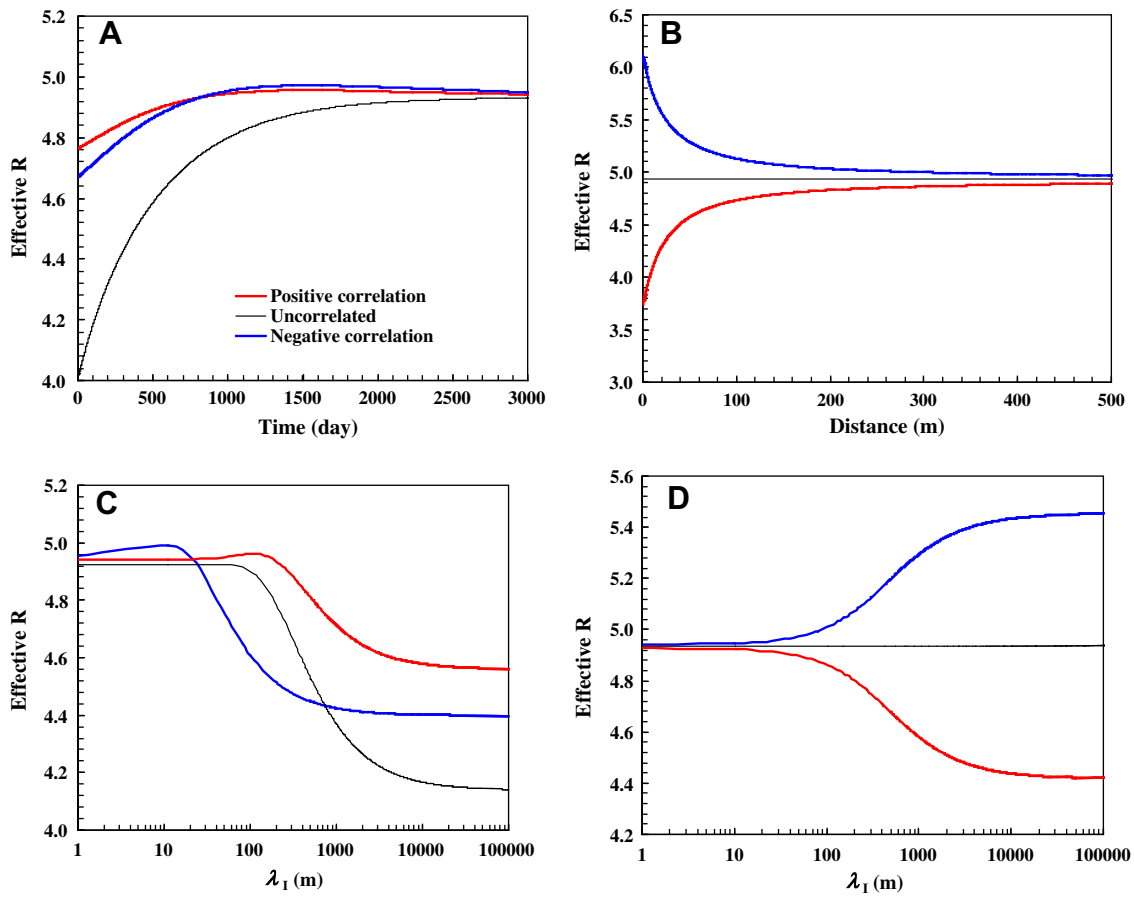

Fig. 2. Time-dependent (A) and scale-dependent (B) effective retardation factor for a porous medium with three RMFs. The time dependent effective retardation factors (C) change with indicator correlation length when time is fixed at 1000 d. The scale-dependent effective retardation factors (D) change with indicator correlation length when lag distance is fixed at 1000 m.

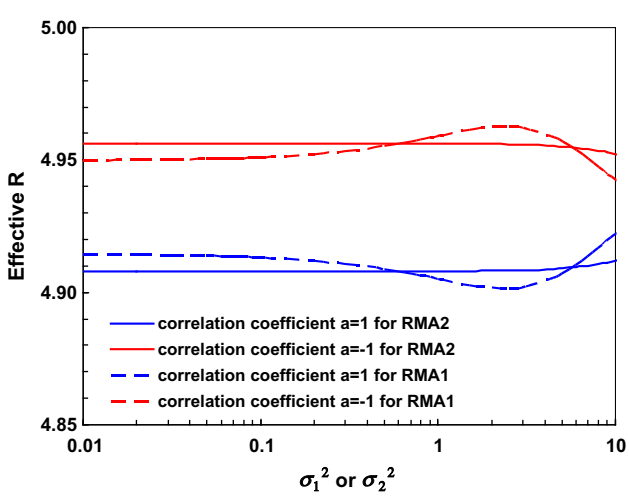

Fig. 3. Scale-dependent effective retardation factor changes with the variance of the hydraulic conductivity for RMA 1 and 2 when the lag distance is fixed at 1000 m and indicator correlation length fixed at 20 m. $a = 1$ and -1 denote a positive and negative correlation, between the hydraulic conductivity and the sorption coefficient, respectively.

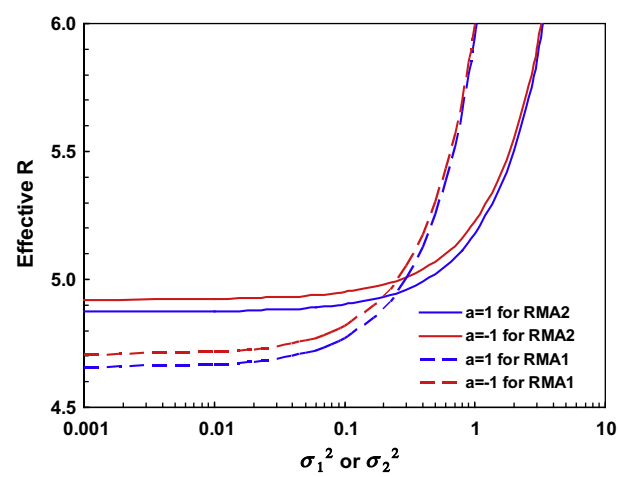

Fig. 4. Scale-dependent effective retardation factor changes with the variances of the sorption coefficients for RMA 1 and 2 when the lag distance is fixed at 1000 m and indicator correlation length fixed at 20 m. $a = 1$ and -1 denote a positive and negative correlation, between the hydraulic conductivity and the sorption coefficient, respectively.

spatial scales are relatively small, scaling effect of the effective retardation factors is relatively large. The chemical heterogeneity has greater influence on scale-dependent effective retardation factor than the physical heterogeneity does. The results from this study provide a methodology to develop effective transport parameters for field-scale modeling at which remediation and risk assessment is actually conducted.

The conceptual model and its corresponding mathematical model derived in this study can be tested with field data or by Monte Carlo simulations, as Deng et al. (2010) did for fractured porous media. On the other hand, because the physical and chemical heterogeneities in aquifer have significant influences on uncertainty quantification of flow and transport (for instance, Ye and Khaleel, 2008; Deng et al., 2009), the conceptual model from this study provides a new one for uncertainty assessment and model selection that requires multiple different conceptual models (Ye et al., 2008) for heterogeneous porous media.

The methodology developed in this study can be applied to non-stationary porous media with hierarchical mineral distribution. Upscaling from RMA to RMF, even to assemblage of RMF is equivalent to classic stochastic upscaling approach from the local to the regional scale. Our upscaling procedure bridges lab bench scale to field scale through quantitatively linking multimodal reactive mineral distribution with scale-dependence of parameters. Therefore, our methodology provides new insights into the origin of the effective retardation factor and has significant practical implications in reactive transport modeling at field scale.

Acknowledgements

The reported research was supported by Los Alamos National Laboratory's Directed Research and Development Project (Number 20070441ER). The fourth author is supported by the DOE project DE-SC0002687 and ORAU/ORNL High Performance Computing Grant. We are grateful to Harihar Rajaram for his constructive comments on this manuscript.

Appendix A. Derivation of spectrum density of fluctuations in ln K

Considering a simple exponential function for autocovariance of $\ln K$, that is:

$$C_{ff}(\xi) = \sigma_f^2 e^{-\frac{\xi}{\lambda}} \tag{A1}$$

The spectrum density S_{ff} of fluctuations in $\ln K$ is evaluated by taking the Fourier transform of Eq. (9). Substituting A1 into Eq. (9), then it yields:

$$S_{ff}(\mathbf{k}) = \frac{1}{(2\pi)^3}\iiint_{-\infty}^{\infty} e^{-i\mathbf{k}\cdot\xi}\sigma_f^2 e^{-\frac{\xi}{\lambda}} d\xi \tag{A2}$$

Integration of A2 is implemented in a spherical coordinate system. The scalar product $\mathbf{k}\cdot\xi = k\xi\cos\theta$, where θ is the angle between wave number vector $\mathbf{k}$ and the separation vector ξ. Expressing the element volume $d\xi$ in spherical coordinates (ξ, θ, α), and integrating A2 results in:

$$\begin{aligned} S_{ff}(\mathbf{k}) &= \frac{1}{(2\pi)^3}\int_{\xi=0}^{\infty}\int_{\theta=0}^{\pi}\int_{\alpha=0}^{2\pi}\sigma_f^2 e^{-\frac{\xi}{\lambda}} e^{-ik\xi\cos\theta}\xi^2\sin\theta d\alpha d\theta d\xi \\ &= \frac{\sigma_f^2\lambda^3}{\pi^2(1+k^2\lambda^2)} \end{aligned} \tag{A3}$$

A3 is the spectrum density for unimodal porous media. For the multimodal porous media, the multimodal covariance function of $\ln K$ (Eq. (10)) is easily integrated to obtain corresponding spectrum density (Eq. (11)) by using A3 three times for three exponential terms.

Appendix B. Derivation of cross-covariance of v1 and R (Eq. (12))

Continue to consider the unimodal porous media from above; its cross-covariance can be expressed as below by substituting A3 into Eq. (8), then taking Fourier transform of (8) and integrating result in

$$C_{v_1R}(\xi) = \frac{\rho_b}{n^2}K_d^G K^G Ja\int\int_{-\infty}^{\infty}\int e^{i\mathbf{k}\cdot\xi}\left(1-\frac{k_1^2}{k^2}\right)\frac{\sigma_f^2\lambda^3}{\pi^2(1+k^2\lambda^2)^2}d\mathbf{k} \tag{B1}$$

Set I is equal to the integration term of B1, then

$$I = \iiint_{-\infty}^{\infty} e^{i\mathbf{k}\cdot\xi}\left(1-\frac{k_1^2}{k^2}\right)\frac{\sigma_f^2\lambda^3}{\pi^2(1+k^2\lambda^2)^2}d\mathbf{k} \tag{B2}$$

Now changing to spherical coordinate system and defining:

$$k_1 = k\cos\beta \tag{B3}$$

$$k_1/k = \cos\theta\cos x + \sin\theta\sin x\cos\alpha \tag{B4}$$

$$dk_1dk_2dk_3 = k^2\sin\theta dk\,d\alpha\,d\theta \tag{B5}$$

where x is the angle between the separation vector ξ and the direction of mean flow k_1, and θ is the angle between ξ and $\mathbf{k}$. Note that the x and ξ stand for coordinates of the autocovariance function, whereas k, θ, and α are spherical coordinates in wave number space. Substitute B3, B4 and B5 into B2, it yields:

$$\begin{aligned} I = \frac{\sigma_f^2}{\lambda\pi^2}\int_{k=0}^{\infty}\int_{\alpha=0}^{2\pi}\int_{\theta=0}^{\pi}\Big\{\Big[&1-\cos^2\theta\cos^2 x-\sin^2\theta\sin^2 x\cos^2\alpha \\ &-2\cos\theta\cos x\sin\theta\sin x\cos\alpha\Big]\frac{k^2\lambda^4}{(1+k^2\lambda^2)^2}e^{ik\xi\cos\theta}\sin\theta dk d\theta d\alpha\Big\} \end{aligned} \tag{B6}$$

Let $\cos\theta = y$ and use the relation of $e^{ik\xi y} = \cos k\xi y + i\sin k\xi y$, B6 becomes B7 after several steps of operation:

$$\begin{aligned} I = &\frac{\sigma_f^2}{\lambda\pi^2}\int_{k=0}^{\infty}\int_{\alpha=0}^{2\pi} \\ &\times\int_{y=-1}^{1}\left\{\left[(1-y^2\cos^2 x)-(1-y^2)\sin^2 x\cos^2\alpha\right]\frac{k^2\lambda^4}{(1+k^2\lambda^2)^2}\cos k\xi y\right\}dk dy d\alpha \end{aligned} \tag{B7}$$

in which we have several integrations below:

$$I_a = \int_0^{\infty}\frac{k^2\lambda^4}{(1+k^2\lambda^2)^2}\cos k\xi y dk = \frac{\pi}{4}\lambda\left(1-\frac{|\xi y|}{\lambda}\right)e^{-\frac{|\xi y|}{\lambda}} \tag{B8}$$

$$I_b = \int_0^{2\pi}(1-y^2)\sin^2 x\cos^2\alpha d\alpha = \pi(1-y^2)\sin^2 x \tag{B9}$$

$$\begin{aligned} I_c &= \int_0^{2\pi}(1-y^2\cos^2 x)d\alpha = 2\pi(1-y^2\cos^2 x) \\ &= \pi(2-2y^2\cos^2 x) \end{aligned} \tag{B10}$$

Of them, B8 can be found from Dwight (1961, p225: definite integral 859.013). Substituting B8, B9 and B10 into B7 yields:

$$\begin{aligned} I = &\frac{\sigma_f^2}{4} \\ &\times\int_{y=-1}^{1}\left\{[2-2y^2\cos^2 x-(1-y^2)\sin^2 x]\left(1-\frac{|\xi y|}{\lambda}\right)e^{-\frac{|\xi y|}{\lambda}}\right\}dy \end{aligned} \tag{B11}$$

Expanding B11 results in

$$I = \frac{\sigma_f^2}{2}\left\{\int_0^1 (1+\cos^2 x)e^{-\frac{\xi y}{\lambda}}dy + \int_0^1 (1-3\cos^2 x)y^2 e^{-\frac{\xi y}{\lambda}}dy - \int_0^1 \frac{\xi}{\lambda}(1+\cos^2 x)ye^{-\frac{\xi y}{\lambda}}dy - \int_0^1 \frac{\xi}{\lambda}(1-3\cos^2 x)y^3 e^{-\frac{\xi y}{\lambda}}dy\right\} = \frac{\sigma_f^2}{2}(I_1 + I_2 - I_3 - I_4) \quad \text{(B12)}$$

In B12 the four integrations I_1, I_2, I_3 and I_4 are given below

$$I_1 = \int_0^1 (1+\cos^2 x)e^{-\frac{\xi y}{\lambda}}dy = -\frac{\lambda}{\xi}(1+\cos^2 x)\left(e^{-\frac{\xi}{\lambda}} - 1\right) \quad \text{(B13)}$$

$$I_2 = \int_0^1 (1-3\cos^2 x)y^2 e^{-\frac{\xi y}{\lambda}}dy = (3\cos^2 x - 1)\left[\left(\frac{\lambda}{\xi}\right)e^{-\frac{\xi}{\lambda}} + 2\left(\frac{\lambda}{\xi}\right)^2 e^{-\frac{\xi}{\lambda}} + 2\left(\frac{\lambda}{\xi}\right)^3\left(e^{-\frac{\xi}{\lambda}} - 1\right)\right] \quad \text{(B14)}$$

$$I_3 = \int_0^1 \frac{\xi}{\lambda}(1+\cos^2 x)ye^{-\frac{\xi y}{\lambda}}dy = -(1+\cos^2 x)\left[e^{-\frac{\xi}{\lambda}} + \frac{\lambda}{\xi}\left(e^{-\frac{\xi}{\lambda}} - 1\right)\right] \quad \text{(B15)}$$

$$I_4 = \int_0^1 \frac{\xi}{\lambda}(1-3\cos^2 x)y^3 e^{-\frac{\xi y}{\lambda}}dy = (3\cos^2 x - 1)\left[e^{-\frac{\xi}{\lambda}} + 3\left(\frac{\lambda}{\xi}\right)e^{-\frac{\xi}{\lambda}} + 6\left(\frac{\lambda}{\xi}\right)^2 e^{-\frac{\xi}{\lambda}} + 6\left(\frac{\lambda}{\xi}\right)^3(e^{-\frac{\xi}{\lambda}} - 1)\right] \quad \text{(B16)}$$

Substituting B13, B14, B15, and B16 into B12, which in turn goes into B1, finally turns out:

$$C_{v_1R}(\xi) = \frac{\rho_b}{2n^2}K_d^G K^G Ja\sigma_f^2\left\{(1+\cos^2 x)e^{-\frac{\xi}{\lambda}} + (1-3\cos^2 x) \times \left[e^{-\frac{\xi}{\lambda}} + 2\left(\frac{\lambda}{\xi}\right)e^{-\frac{\xi}{\lambda}} + 4\left(\frac{\lambda}{\xi}\right)^2 e^{-\frac{\xi}{\lambda}} + 4\left(\frac{\lambda}{\xi}\right)^3(e^{-\frac{\xi}{\lambda}} - 1)\right]\right\} \quad \text{(B17)}$$

When the separation vector is parallel to the flow direction, $x = 0$, $\cos x = 1$, then:

$$C_{v_1R}(\xi) = \frac{\rho_b}{n^2}K_d^G K^G Ja\sigma_f^2\left[4\left(\frac{\lambda}{\xi}\right)^3(1 - e^{-\frac{\xi}{\lambda}}) - 4\left(\frac{\lambda}{\xi}\right)^2 e^{-\frac{\xi}{\lambda}} - 2\left(\frac{\lambda}{\xi}\right)e^{-\frac{\xi}{\lambda}}\right] \quad \text{(B18)}$$

Let $\xi \to 0$, the cross-variance of v_1 and R for unimodal porous media can be given below:

$$\sigma_{v_1R}^2 = C_{v_1R}(0) = \frac{2\rho_b}{3n^2}K_d^G K^G Ja\sigma_f^2 \quad \text{(B19)}$$

Using the same integration method for multimodal porous media, the corresponding multimodal cross-covariance function (Eq. (12)) can be obtained by using B18 three times for three exponential terms.

In a similar way the covariance function of flow velocity (v_1) for unimodal porous media can be retrieved as following

$$C_{v_1v_1}(\xi) = \frac{\sigma_f^2(K^G J)^2}{n^2}\left\{\left[8\left(\frac{\lambda}{\xi}\right)^2 + 48\left(\frac{\lambda}{\xi}\right)^3 + 96\left(\frac{\lambda}{\xi}\right)^4\right]e^{-\frac{\xi}{\lambda}} + \left[96\left(\frac{\lambda}{\xi}\right)^5 - 8\left(\frac{\lambda}{\xi}\right)^3\right](e^{-\frac{\xi}{\lambda}} - 1)\right\} \quad \text{(B20)}$$

The variance of flow velocity (v_1) for unimodal porous media is obtained when separation distance $\xi \to 0$, that is:

$$\sigma_{v_1}^2 = C_{v_1v_1}(0) = \frac{8}{15}\frac{\sigma_f^2(K^G J)^2}{n^2} \quad \text{(B21)}$$

For multimodal porous media the covariance function of flow velocity (Eq. (14)) can also be gained in a similar integration procedure used above.

Appendix C. Derivation of equation for space dependent effective retardation factor

For a passive or conservative particle, retardation factor R is equal to 1. Eq. (21) is then reduced into one below:

$$\frac{dT_p}{dx} = \frac{1}{\bar{v}_1}\left[1 + \frac{1}{\bar{v}_1^2}C_{v_1v_1}(x,0,0)\right] \quad \text{(C1)}$$

Substituting B20 into C1 and integrating C1, it brings out the travel time of the passive particle in unimodal porous media as:

$$T_p = \int_0^x \frac{1}{\bar{v}_1}\left[1 + \frac{1}{\bar{v}_1^2}C_{v_1v_1}(x,0,0)\right]dx = \frac{x}{\bar{v}_1} + \frac{(K^G J)^2\lambda\sigma_f^2}{\bar{v}_1^3 n^2}\left\{24\left(\frac{\lambda}{x}\right)^4 \times (1 - e^{-\frac{x}{\lambda}}) - 24\left(\frac{\lambda}{x}\right)^3 e^{-\frac{x}{\lambda}} - 4\left(\frac{\lambda}{x}\right)^2(1 + 2e^{-\frac{x}{\lambda}}) + 1\right\} \quad \text{(C2)}$$

For a sobbing particle, substituting B18 and B20 into Eq. (21), and then integrating yields:

$$T = \int_0^x \frac{\bar{R}}{\bar{v}_1}\left[1 + \frac{1}{\bar{v}_1^2}C_{v_1v_1}(x,0,0) - \frac{1}{\bar{R}\bar{v}_1}C_{Rv_1}(x,0,0)\right]dx = \bar{R}T_p - \frac{\rho_b K_d^G K^G Ja\lambda\sigma_f^2}{n^2\bar{v}_1^2}\left\{2\left(\frac{\lambda}{x}\right)^2(e^{-\frac{x}{\lambda}} - 1) + 2\left(\frac{\lambda}{x}\right)e^{-\frac{x}{\lambda}} + 1\right\} \quad \text{(C3)}$$

For multimodal porous media, similar integrations can be completed as shown in Eqs. (22) and (23).

References

Allen-King, R.M., Halket, R.M., Gaulord, D.R., Robin, M.J.L., 1998. Charactering the heterogeneity and correlation of perchloroethene sorption and hydraulic conductivity using a facies-based approach. Water Resour. Res. 34 (3), 385–396.

Allen-King, R.M., Divine, D.P., Robin, M.J.L., Alldredge, J.R., Gaylord, D.R., 2006. Spatial distributions of perchloroethylene reactive transport parameters in the Borden Aquifer. Water Resour. Res. 42, W01413. http://dx.doi.org/10.1029/2005WR003977.

Attinger, S., Dentz, M., Kinzelbach, H., Kinzelbach, W., 1999. Temporal behavior of a solute cloud in a chemically heterogeneous porous medium. J. Fluid Mech. 386, 77–104.

Bellin, A., Rinaldo, A., Bosma, W.J.P., van Der Zee, S.E.A.T.M., Rubin, Y., 1993. Linear equilibrium adsorbing solute transport in physically and chemically heterogeneous porous formations: 1. Analytical solutions. Water Resour. Res. 29 (12), 4019–4030.

Berkowitz, B., Cortis, A., Dentz, M., Scher, H., 2006. Modeling non-Fickian transport in geological formations as a continuous time random walk. Rev. Geophys. 44, RG2003, doi: 10.1029/2005RG000178.

Bolster, D., Dentz, M., 2012. Anomalous dispersion in chemically heterogeneous media induced by long range correlations. J. Fluid Mech. 695, 366–389.

Cheng, T., Barnett, M.O., Roden, E.E., Zhuang, J., 2007. Reactive transport of uranium (VI) and phosphate in a goethite-coated sand column: an experimental study. Chemosphere 68 (7), 1218–1223.

Chrysikopoulos, C.V., Kitanidis, P.K., Roberts, P.V., 1990. Analysis of one-dimensional solute transport through porous media with spatially variable retardation factor. Water Resour. Res. 26 (3), 437–446.

Cvetkovic, V., Dagan, G., 1994. Transport of kinetically sorbing solute by steady random velocity in heterogeneous porous formations. J. Fluid Mech. 265, 189–215.

Dagan, G., Svetkovic, V., Shapiro, A., 1992. A solute approach to transport in heterogeneous formations, 1. The general framework. Water Resour. Res. 28 (5), 1369–1376.

Dai, Z., Ritzi, R.W., Huang, C., Rubin, Y.N., Dominic, D.F., 2004. Transport in heterogeneous sediments with multimodal conductivity and hierarchical organization across scales. J. Hydrol. 294 (1–3), 68–86.

Dai, Z., Wolfsberg, A.V., Lu, Z., Ritzi, R.W., 2007a. Representing aquifer architecture in macrodispersivity models with an analytical solution of the transition probability matrix. Geophys. Res. Lett. 34, L20406. http://dx.doi.org/10.1029/2007GL031608.

Dai, Z., Wolfsberg, A.V., Lu, Z., Reimus, P., 2007b. Upscaling matrix diffusion coefficients for heterogeneous fractured rocks. Geophys. Res. Lett. 34, L07408. http://dx.doi.org/10.1029/2007 GL029332.

Dai, Z., Wolfsberg, A.V., Lu, Z., Deng, H., 2009. Scale dependence of sorption coefficients for radionuclide transport in saturated fractured rock. Geophys. Res. Lett. 36, L01403. http://dx.doi.org/10.1029/2008GL036516.

Davis, J.A., Yabusaki, S.B., Steefel, C.I., Zachara, J.M., Curtis, G.P., Redden, G.D., Criscenti, L.J., Honey, B.D., 2004. Assessing conceptual models for subsurface reactive transport of inorganic contaminants. Trans. Am. Geophys. Union, EOS 85(44), November 2.

Deng, H., Ye, M., Schaap, M.G., Khaleel, R., 2009. Quantification of uncertainty in pedotransfer function-based parameter estimation for unsaturated flow modeling. Water Resour. Res. 45, W04409. http://dx.doi.org/10.1029/2008WR007477.

Deng, H., Dai, Z., Wolfsberg, A.V., Lu, Z., Ye, M., Reimus, P., 2010. Upscaling of reactive mass transport in fractured rocks. Water Resour. Res. 46, W06501, doi: 10.1029/2009 WR008363.

Dentz, M., Cortis, A., Scher, H., Berkowitz, B., 2004. Time behavior of solute transport in heterogeneous media: Transition from anomalous to normal transport, Adv. Water Resour. 27, 155–173. http://dx.doi.org/10.1016/j.advwatres.2003.11.002.

Dentz, M., Boster, D., 2010. Distribution- versus correlation-induced anomalous transport in quenched random velocity fields. Phys. Res. Lett. 105, 244301. http://dx.doi.org/10.1103/PhysRevLett. 105.244301.

Dentz, M., Castro, A., 2009. Effective transport dynamics in porous media with heterogeneous retardation properties. Geophys. Res. Lett. 36, L03403. http://dx.doi.org/10.1029/2008 GL036846.

Dwight, H.B., 1961. Tables of Integrals and Other Mathematical Data, p225, fourth ed. The Macmillan Company, New York.

Fernàndez-Garcia, D., Illangasekare, T.H., Rajaram, H., 2005. Differences in the scale dependence of dispersivity and retardation factors estimated from forced-gradient and uniform flow tracer tests in three-dimensional physically and chemically heterogeneous porous media. Water Resour. Res. 41, W03012. http://dx.doi.org/10.1029/2004WR003125.

Gelhar, L.W., 1993. Stochastic Subsurface Hydrology. Prentice-Hall, Englewood Cliffs, NJ.

Liu, C., Zachara, J.M., Qafoku, N.P., Wang, Z., 2008. Scale-dependent desorption of uranium from contaminated subsurface sediments. Water Resour. Res. 44, W08413. http://dx.doi.org/10.1029/2007 WR006478.

Rajaram, H., 1997. Time and scale dependent effective retardation factors in heterogeneous aquifers. Adv. Water Resour. 20 (4), 217–230.

Ritzi, W.R., Dai, Z., Dominic, D.F., Rubin, Y.N., 2004. Spatial correlation of permeability in cross-stratified sediment with hierarchical architecture. Water Resour. Res. 40, W03513. http://dx.doi.org/10.1029/2003WR002420.

Rubin, Y., 2003. Applied Stochastic Hydrogeology. Oxford Univ. Press, New York.

Russo, A., Johnson, G.R., Schnaar, G., Brusseau, M.L., 2010. Nonideal transport of contaminants in heterogeneous porous media: 8. Characterizing and modeling asymptotic contaminant-elution tailing for several soils and aquifer sediments. Chemosphere 81, 366–371.

Ye, M., Khaleel, R., 2008. A Markov chain model for characterizing medium heterogeneity and sediment layering structure. Water Resour. Res. 44, W09427. http://dx.doi.org/10.1029/2008 WR006924.

Ye, M., Mayer, P.D., Neuman, S.P., 2008. On model selection criteria in multimodel analysis. Water Resour. Res. 44, W03428. http://dx.doi.org/10.1029/2008WR006803.